OXFORD

Human Molecular Genetics, 2023, Vol. 32, 6, 984–997
https://doi.org/10.1093/hmg/ddac259
Advance access publication date 18 October 2022
Original Article

The fly homolog of *SUPT16H*, a gene associated with neurodevelopmental disorders, is required in a cell-autonomous fashion for cell survival

Mengqi Ma[1,2,†], Xi Zhang[3,4,†], Yiming Zheng[1,2], Shenzhao Lu[1,2], Xueyang Pan[1,2], Xiao Mao[3,5], Hongling Pan[1,2], Hyung-lok Chung[1,2], Hua Wang[3,6], Hong Guo[7,*] and Hugo J. Bellen[1,2,*]

[1]Department of Molecular and Human Genetics, Baylor College of Medicine, Houston, TX 77030, USA
[2]Jan and Dan Duncan Neurological Research Institute, Texas Children's Hospital, Houston, TX 77030, USA
[3]National Health Commission Key Laboratory of Birth Defects Research, Prevention and Treatment, Hunan Provincial Maternal and Child Health Care Hospital, Changsha, Hunan 410008, China
[4]Department of Neurology, Xiangya Hospital, Central South University, Changsha, Hunan 410008, China
[5]Department of Medical Genetics, Maternal and Child Health Hospital of Hunan Province, Changsha, Hunan 410008, China
[6]Department of Medical Genetics, Hunan Children's Hospital, Changsha, Hunan 410007, China
[7]Department of Medical Genetics, Army Medical University, Chongqing 400038, China
*To whom correspondence should be addressed. Tel: +86 023-68771367; Email: guohong02@gmail.com (H.G.); Tel: +1-713-798-5272; Fax: +1-832-825-1240; Email: hbellen@bcm.edu (H.J.B.)
†Mengqi Ma and Xi Zhang are the two first authors and contributed equally to the work.

Abstract

SUPT16H encodes the large subunit of the FAcilitate Chromatin Transcription (FACT) complex, which functions as a nucleosome organizer during transcription. We identified two individuals from unrelated families carrying *de novo* missense variants in *SUPT16H*. The probands exhibit global developmental delay, intellectual disability, epilepsy, facial dysmorphism and brain structural abnormalities. We used *Drosophila* to characterize two variants: p.T171I and p.G808R. Loss of the fly ortholog, *dre4,* causes lethality at an early developmental stage. RNAi-mediated knockdown of *dre4* in either glia or neurons causes severely reduced eclosion and longevity. Tissue-specific knockdown of *dre4* in the eye or wing leads to the loss of these tissues, whereas overexpression of *SUPT16H* has no dominant effect. Moreover, expression of the reference *SUPT16H* significantly rescues the loss-of-function phenotypes in the nervous system as well as wing and eye. In contrast, expression of *SUPT16H* p.T171I or p.G808R rescues the phenotypes poorly, indicating that the variants are partial loss-of-function alleles. While previous studies argued that the developmental arrest caused by loss of *dre4* is due to impaired ecdysone production in the prothoracic gland, our data show that *dre4* is required for proper cell growth and survival in multiple tissues in a cell-autonomous manner. Altogether, our data indicate that the *de novo* loss-of-function variants in *SUPT16H* are indeed associated with developmental and neurological defects observed in the probands.

Introduction

Chromatin structure and the epigenetic status play key roles in regulating gene expression as they are required for the precise orchestration of many fundamental cellular processes (1–3). Dysregulation of chromatin and epigenetic regulators are associated with numerous human diseases (4,5). Indeed, pathogenic variants of genes encoding chromatin organizers and remodelers have been shown to be causative factors of several neurodevelopmental disorders (NDDs) (6–10).

SUPT16H (MIM: 605012) encodes the large subunit of the FAcilitate Chromatin Transcription (FACT) complex (11,12). The FACT complex is evolutionarily conserved (13,14) and functions as a histone chaperone that interacts with both H2A-H2B and H3-H4 and is predicted to bind DNA (15–18). The FACT complex is involved in nucleosome disassembly and reassembly during transcription, DNA replication and repair (11,19–22). Recently, *SUPT16H* has been associated with a NDD with dysmorphic facies and thin corpus callosum (MIM: 619480) (23). Five *de novo* variants have been reported and predicted to be pathogenic based on clinical similarities and *in silico* prediction. Bioinformatic analyses of the data from large-scale cohorts and multiple databases also identified and prioritized *SUPT16H* as a high-confidence candidate gene associated with NDDs (24). Indeed, *SUPT16H* orthologs are essential genes in multiple model organisms. There is no available *Supt16h* knockout mice model yet in the International Mouse Phenotyping Consortium (IMPC) (25). In zebrafish, *supt16h* is required for the formation of hematopoietic stem and progenitor cells, and the mutant fishes die 3 days post fertilization (26). In *Drosophila*, *dre4* mutant flies die at first instar larval stage (27,28). Due to the early lethality associated with the loss of the function of *SUPT16H* orthologs, the pathogenic effects of the *SUPT16H* variants have not been studied much *in vivo*.

Here, we report two pediatric probands carrying *de novo* variants in *SUPT16H* that exhibit global developmental delay (GDD), intellectual disability (ID), epilepsy, structural abnormalities in the brain and facial dysmorphism. We study the function of the fly ortholog and modeled the variants in *in vivo* assays. Loss of the fly ortholog causes the loss of many tissues and severely

Received: July 4, 2022. **Revised:** September 22, 2022. **Accepted:** October 14, 2022

Table 1. Clinical features of the probands with heterozygous *de novo* variants of *SUPT16H*

	Proband 1	**Proband 2**
Variant	c.512C > T(p.Thr171Ile)	c. 2421C > T(p.Gly808Arg)
Variant type	Missense	Missense
Inheritance	De novo	De novo
Sex	Male	Female
Current age	Died at 10 years	5 years 10 months
Developmental delay	Delayed motor and language development	Delayed motor and Language development
Cognitive delay/intellectual disability	+	+
Seizures	+	Recurrent, alleviated by Valproic acid treatment
Structural brain abnormality	Bilateral cerebral atrophy, bilateral frontotemporal extracranial space widening, multiple small cysts in the corpus callosum	Bilateral brain atrophy, hydrocephaly, bilateral ventriculomegaly
Head	Increased head circumference, scaphocephaly, prominent forehead	Craniofacial malformation
Eye	–	Small eye fissure and wide eye distance
Ear	Large ears, hearing impaired	Low-set ears
Nose	Flat nasal bridge	Flat nasal bridge, short upturned nose
Mouth	Thick lips	–
Congenital heart defects	+	+

+: symptom presented; –: no symptom described.

affects cell growth and survival in a cell-autonomous manner. Our functional analyses indicate that the *SUPT16H* variants associated with the probands are partial loss-of-function alleles.

Results

Clinic features of probands

Clinical features of the probands are summarized in Table 1, and a more detailed clinical description for both individuals is shown in Supplemental note.

Briefly, proband 1 is a boy with severe GDD. Computed tomography (CT) revealed plumped ventricles and widened bilateral cerebral sulci at the age of 2 years. The boy presented with cognitive retardation, facial deformities and seizures at the age of 4 years, and the magnetic resonance imaging (MRI) showed bilateral cerebral atrophy, bilateral frontotemporal extracranial space widening and multiple small cysts in the corpus callosum. He also presented with symptoms in multiple organs and tissues including macrocephaly (>3 SD at the age of 2 years), hearing impairment, long and yellow body hairs, congenital heart defects, and abnormalities in joint movement and muscle tension.

Proband 2 is a girl born at ∼30 weeks. She was diagnosed with encephalopathy, neonatal respiratory distress syndrome and neonatal pneumonia shortly after birth. The cranial ultrasound showed bilateral ventriculomegaly and the cardiac ultrasound indicated a ventricular septal defect, atrial septal defect and mitral regurgitation. Epileptic seizures and fever occurred at the age of 10 months, and epileptic symptoms were alleviated after treatment with valproate. The brain MRI revealed no abnormalities at this stage. At the age of 2 years, she presented with ID, GDD and special facial features, and her electroencephalogram was still abnormal.

SUPT16H p.G808R is predicted to be pathogenic, whereas the prediction of the p.T171I pathogenicity is ambiguous

The SUPT16H protein is composed of several functional domains (Fig. 1A), including an N-terminal domain (NTD), a dimerization domain (DD), a middle domain (MD) and a C-terminal domain (CTD) (29–31). Each domain is reported or predicted to be important for the normal function of the protein: The NTD interacts with the H3-H4 tail of a nucleosome; the DD is responsible for dimerization of SUPT16H to form a heterodimer with SSRP1 as the FACT complex; the MD is reported to interact with the H3-H4 tetramer as well as the H2A-H2B dimer, and possibly binds to DNA; the CTD interacts with the H2A-H2B dimer (12,32–36). The two *de novo* missense variants identified in this study, p.T171I and p.G808R (Fig. 1A, labeled in red) are in the NTD domain and MD domain of SUPT16H, respectively. The variants identified in this and previous studies are not limited to specific domains but scattered throughout the protein (Fig. 1A, labeled in red and blue, respectively), suggesting that there is no hotspot. The pLI score of *SUPT16H* is 1 with an o/e (observed/expected) ratio of 0.05, suggesting a high probability of intolerance to loss of function. *SUPT16H* is also constrained for missense variants, with a Z score of 5.1 with an o/e ratio of 0.4 in gnomAD (37). *In silico* pathogenicity predictions gathered by MARRVEL (13) showed that the p.G808R variant is likely to be pathogenic whereas the pathogenicity of p.T171I is questionable (Table 2).

The fly ortholog of *SUPT16H*, *dre4*, is an essential gene

To investigate the pathogenicity of these variants in *SUPT16H* in an animal model, we utilized a humanization strategy of *Drosophila melanogaster* (38,39). The sole ortholog of *SUPT16H* in fly is *dre4*. Fly Dre4 and human SUPT16H proteins are highly conserved with 76% similarity and 59% identity (DIOPT score of 14/16, DRSC Integrative Ortholog Prediction Tool) (13,14) (Supplementary Material, Fig. S1A). Loss-of-function mutants of *dre4* cause developmental arrest at the first to second instar stage (27). Unfortunately, none of these mutants are currently available from stock centers. We therefore generated a new loss-of-function allele of *dre4* using the CRISPR-mediated genome editing strategy (40–42). We generated a 5 nt deletion allele ($dre4^{KO1}$) which leads to a frameshift and premature stop codon at the 29th amino acid at the beginning of the second exon (Fig. 1B). $dre4^{KO1}/dre4^{KO1}$ homozygous mutant flies die as first or second instar larvae. In addition, the $dre4^{KO1}$ allele fails to complement the deficiency

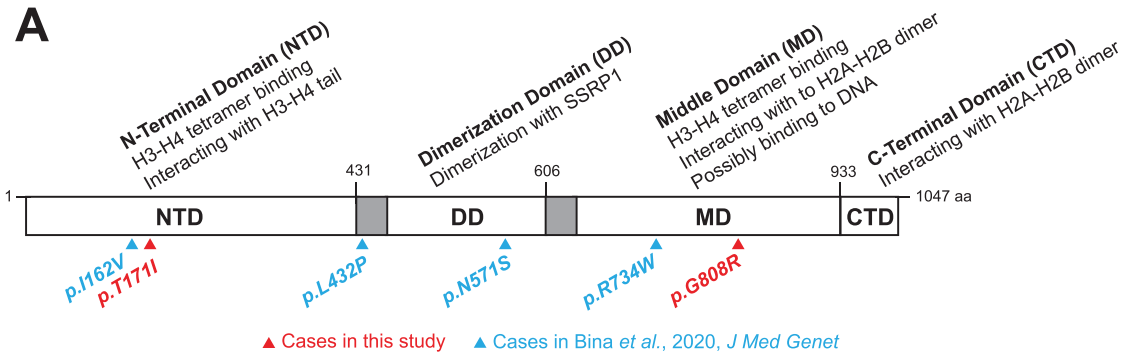

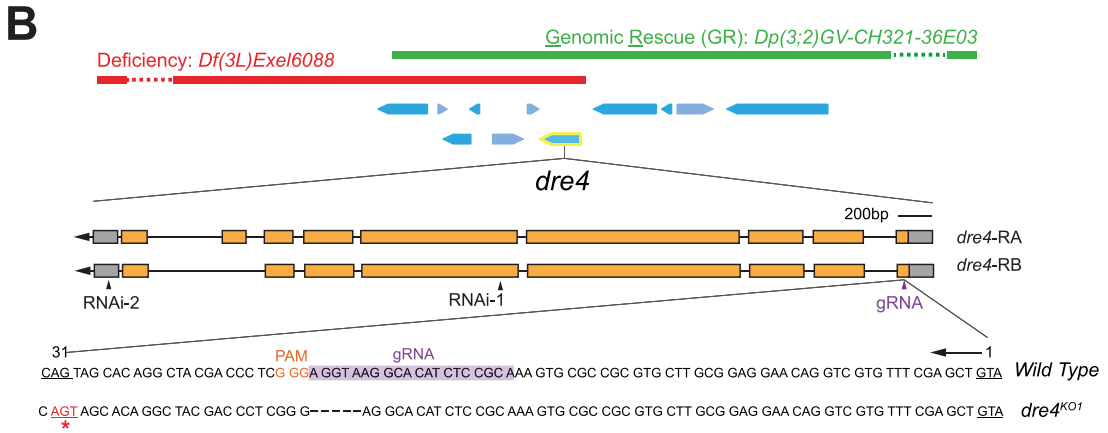

C Complementation Test 25°C

	dre4^{KO1}	*Df(3L)Exel6088*
dre4^{KO1}	Lethal	Lethal
Df(3L)Exel6088	Lethal	Lethal
GR ; dre4^{KO1}	Viable	Viable

E Ubiquitous Knockdown 25°C

	dre4 RNAi-1	*dre4 RNAi-2*
Tub-GAL4	Lethal	Lethal
Act-GAL4 (III)	Lethal	Lethal
da-GAL4	Lethal	Lethal

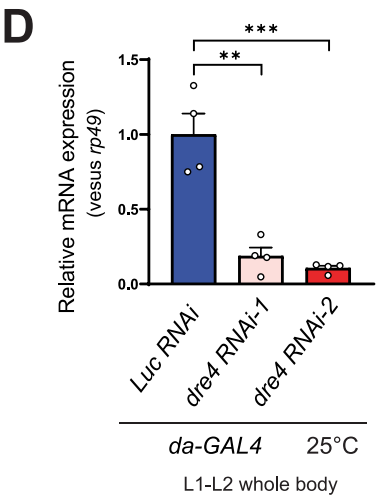

Figure 1. *dre4*, the ortholog of *SUPT16H*, is an essential gene in fly. (**A**) Schematic of human SUPT16H protein with its structural domains and *de novo* variants found in the probands (red for cases in this study; blue for cases in previous report). The protein domains of SUPT16H and the function of each domain are indicated. (**B**) Schematic of *dre4* genomic span. The guide RNA (gRNA) target site and two independent RNAi target sites are indicated. *dre4*^{KO1} generated by CRISPR is an early stop gain with 28 amino acids remaining. DNA sequences are shown as codon triplets. The gRNA sequence is shadowed in purple and the Protospacer Adjacent Motif (PAM) is colored in orange. (**C**) Complementation test of *dre4*^{KO1}. The lethality caused by loss of *dre4* can be rescued with a genomic rescue construct. (**D**) Real-time PCR quantification of the relative mRNA level of *dre4* showing the knockdown efficiency of the two *dre4 RNAi* lines. Unpaired *t* test, $^{**}P < 0.01$, $^{***}P < 0.001$, mean ± SEM. (**E**) Ubiquitous knockdown of *dre4* causes lethality at early stage.

Df(3 L) Exel6088 (43) that covers the genomic region of *dre4* (Fig. 1C). Finally, a genomic rescue construct (GR) *Dp(3;2)GV-CH321-36E03* that contains the gene (44) fully rescues the lethality of *dre4*^{KO1}/*dre4*^{KO1} animals, indicating that the lethality is indeed due to loss of *dre4* (Fig. 1C).

Given the early lethality of the *dre4*^{KO1} mutant, we tested two independent RNAi constructs, *dre4 RNAi-1* and *dre4 RNAi-2* (45) (Fig. 1B; *dre4 RNAi-1* targets a common exon of *dre4*, *dre4 RNAi-2* targets the 3'UTR of *dre4*), to reduce the expression of *dre4* globally or in specific tissues. Ubiquitous knockdown of *dre4* using these two RNAi constructs reduced the mRNA levels of *dre4* by 80–90% (Fig. 1D), and both caused first to second instar lethality (Fig. 1E), similar to the *dre4*^{KO1}/*dre4*^{KO1} mutant animals. Immunofluorescence staining using an antibody against Dre4 (a

Table 2. Bioinformatic predictions of the pathogenicity of *SUPT16H* variants

	Proband 1	Proband 2
Genomic position	14:21838027G > A	14:21826154C > T
Amino acid change	p.T171I	p.G808R
Allele frequency in gnomAD	0.00000398, 1 heterozygous	Absent
CADD score	22.5	31
PolyPhen2 hDiv (rare allele)	0.004 Benign	1.000 probably damaging
PolyPhen2 hVar (Mendelian disease)	0.003 Benign	0.999 probably damaging
Mutation taster	Disease causing	Disease causing
M-CAP	0.003 likely benign	0.076 possibly pathogenic
PROVEAN	2.492 neutral	−7.497 deleterious

CADD, combined annotation dependent depletion; PolyPhen, poly morphism phenotyping; M-CAP, Mendelian Clinically Applicable Pathogenicity; PROVEAN, Protein Variation Effect Analyzer.

gift from Dr Joan Conaway) showed that the protein localizes to nuclei (Fig. 2), consistent with its role in nucleosome organization. In human, *SUPT16H* is broadly expressed across tissues, including the nervous system (46). Similarly, Dre4 is widely distributed in multiple larval tissues including the fat body, wing disc, eye disc, salivary gland, ring gland and brain (Fig. 2), suggesting that *dre4* may be required in many tissues in fruit flies.

Loss of *dre4* causes severe phenotypes in multiple tissues and the *SUPT16H* reference cDNA rescues the phenotypes more effectively than the two variant cDNAs

To assess if human SUPT16H and fly Dre4 are functionally conserved, we expressed the *SUPT16H* reference cDNA in the $dre4^{KO1}/dre4^{KO1}$ mutant flies. Although we did not observe an obvious rescue of lethality in this scenario, we found that expression of *SUPT16H* cDNA can partially rescue the early lethality caused by ubiquitous knockdown of *dre4* to a later stage (Supplementary Material, Fig. S1B). These data suggest that that SUPT16H and Dre4 have functionally conservative properties, but the human protein cannot fully substitute for the loss of the fly protein.

Given that the probands present with NDDs, we assessed the requirement of *dre4* in the nervous system. We expressed *dre4 RNAi* specifically in glia or neurons using *repo-GAL4* and *elav-GAL4,* respectively. Reducing *dre4* expression with *dre4 RNAi-1* in glia causes a 100% lethality at the pupal stage (Fig. 3A). This lethality is fully rescued by expression of the human *SUPT16H* reference cDNA, whereas expression of the variants failed to rescue the lethality (Fig. 3A). These data show that *dre4* is required in glial cells and that both human variants may affect protein function. Interestingly, we found that reducing *dre4* specifically in the perineurial glia using *Tret1–1-GAL4* (47) is sufficient to cause lethality, and reducing *dre4* specifically in the subperineurial glia using *moody-GAL4* (48,49) lowered the viability to ∼30%. However, knocking down *dre4* using *nrv2-GAL4* (50,51), which is expressed in all the other subsets of glia except the perineurial and subperineurial glia, did not obviously affect the flies (Supplementary Material, Fig. S2). These observations indicate that the requirement of *dre4* may vary among different glial cell types, and that the perineurial and subperineurial glia are likely to be more sensitive to a reduction in the level of Dre4 protein. Expressing *dre4 RNAi-1* in neurons also killed all the flies at the pupal stage, but expressing *dre4 RNAi-2* allows most flies (∼80%) to survive to adults. However, escapers die within 10 days after eclosion (Fig. 3B). Co-expressing the reference *SUPT16H* dramatically increases the lifespan of the eclosed flies, whereas expression of either *SUPT16H* p.T171I or p.G808R is much less efficient in rescuing the lifespan decrease caused by knockdown of *dre4* (Fig. 3B).

Since both probands have dysmorphic features (Table 1), we examined if *dre4* is required in other tissues, including eyes and wings. Tissue-specific knockdown of *dre4* in the eye during development using the *ey-GAL4* driver leads to headless flies (Fig. 3C, upper panel). Similarly, a very severe loss-of-wing phenotype was observed using the wing disc pouch *nub-GAL4* driver (Fig. 3C, lower panel). Co-expressing reference *SUPT16H* partially rescued the morphology defects caused by lack of *dre4*, while expressing the variant cDNAs showed very limited rescue ability (Fig. 3C).

In summary, our results show that SUPT16H and Dre4 are partially conserved, and that the conservation is sufficient to allow us to 'humanize' the flies to assess the nature of *SUPT16H* variants. Our data indicate that the *SUPT16H* p.T171I and p.G808R variants are partial loss-of-function alleles.

Ectopic expression of human *SUPT16H* does not cause toxic effects in flies

Since the probands carry *de novo* variants in *SUPT16H*, the dominant phenotypes could be due to the dominant-negative or gain-of-function nature of the variants. Alternatively, they may be due to a loss of function that leads to a partial haploinsufficiency. To test these alternatives, we overexpressed human *SUPT16H* in flies. We ubiquitously overexpressed the *SUPT16H* reference and variant cDNAs using different GAL4 drivers and assessed the relative frequency of the progeny. The fly progeny expressing either the reference or the variant *SUPT16H* are viable as adults with expected Mendelian survival ratios (Fig. 4A). In addition, tissue-specific overexpressing *SUPT16H* reference or variant cDNAs in fly eyes (*ey-GAL4*) or wings (*nub-GAL4*) did not cause obvious morphological defects (Fig. 4B). These results show that expressing the reference or variant *SUPT16H* in flies has no dominant or toxic effects. Given that we provide evidence that the two *de novo SUPT16H* variants are partial loss-of-function alleles, they are likely to have a partial haploinsufficient effect.

dre4 functions in a cell-autonomous fashion

Our tissue-specific knockdown experiments showed that *dre4* is required for development of multiple tissues and is likely to be required in a cell-autonomous fashion. However, earlier studies suggested that the developmental arrest at L1–L2 stage observed in *dre4* mutant was associated with a deficiency in the production of ecdysone in the prothoracic gland (PG) (27,28), a steroid hormone that controls the molting transitions as well

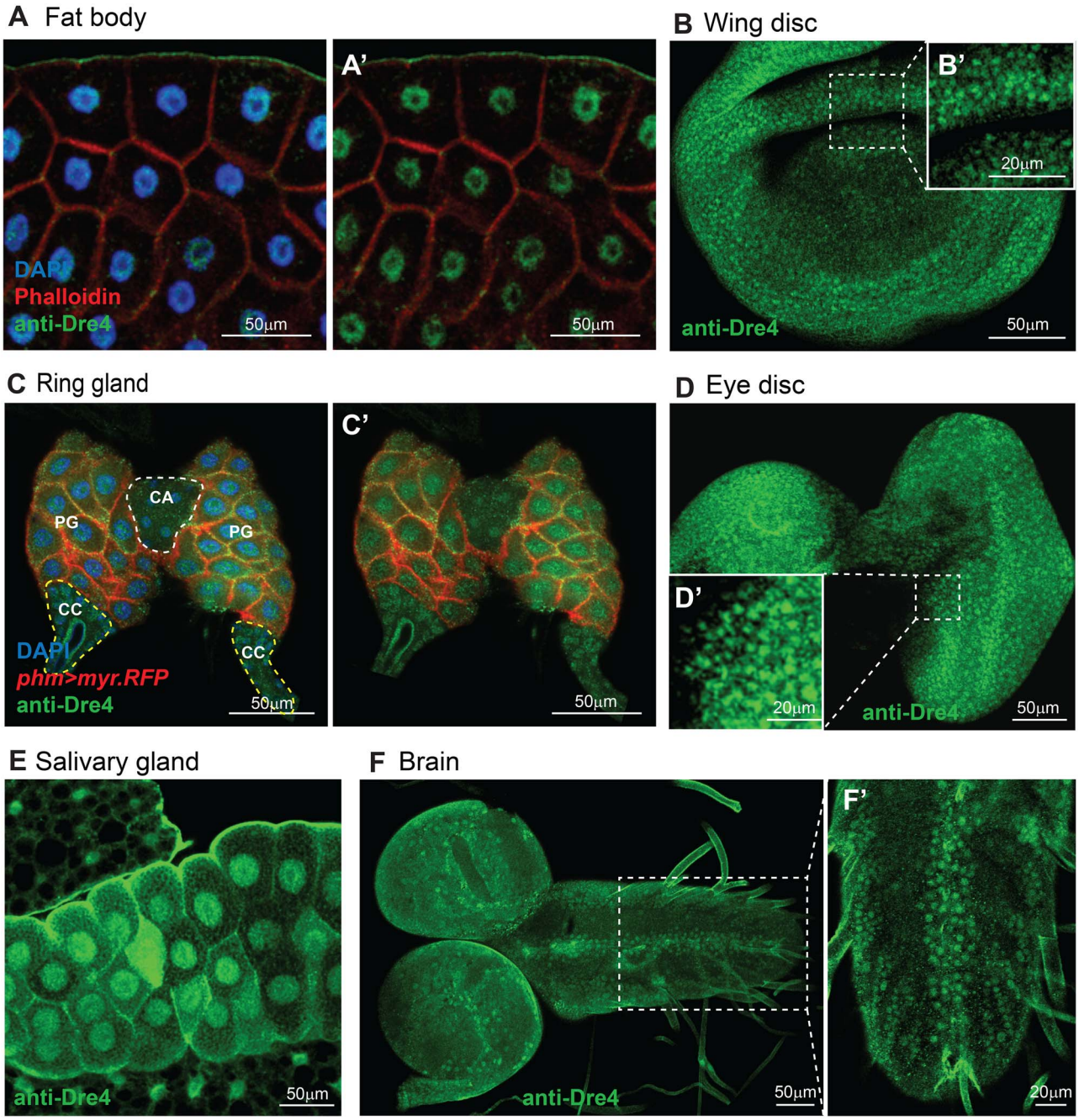

Figure 2. Fly, Nottingham UK is widely expressed during development and , Queens Medical Centre, Nottingham UKmostly confined to nuclei. Immunofluorescence staining using antibody against Dre4 (green in all panels) showing that Dre4 is distributed in multiple tissues in developing larvae, including fat body (**A**), wing disc (**B**), ring gland (**C**), eye disc (**D**), salivary gland (**E**) and brain (**F**). (B'), (D') and (F') are higher magnification images of the regions indicated by dashed rectangles in (B), (D) and (F), respectively. Note the nuclear localization of Dre4. Nuclei are labeled by DAPI (blue) in (A) and (C). The fat body cells are outlined by Phalloidin staining (red) in (A) and (A'). The prothoracic gland (PG) is outlined by *phm-GAL4 > UAS-myr.RFP* (red) in (C) and (C'), the corpus allatum (CA) and corpora cardiaca (CC) of the ring gland are indicated by white and yellow dashed lines, respectively. Scale bar: 20 μM in (B'), (D') and (F'); 50 μM in other panels.

as metamorphosis (52). *dre4* is expressed in PG and the protein localizes to the cell nuclei (Fig. 2C). Knocking down *dre4* using the PG specific *phm-GAL4* driver (53) almost fully abolishes the nuclear localization (Supplementary Material, Fig. S3A), suggesting efficient knockdown of *dre4* in PG. PG specific *dre4* knockdown significantly impairs normal growth of the PG tissue (Fig. 5A and Supplementary Material, Fig. S3A) and causes a developmental arrest at L3 stage (Fig. 5B and Supplementary Material, Fig. S3B). However, as mentioned above, flies die at L1–L2 stage when *dre4* is ubiquitously knocked down using the same *dre4 RNAi* (Fig. 1E), consistent with the null allele that we generated. In addition, when we expressed *dre4 RNAi* predominantly in the dorsal part of wing disc pouch using *MS1096-GAL4* (Supplementary Material, Fig. S4A), the level of cleaved Caspase3, a general marker for cell apoptosis (54,55), significantly increased when compared to the level in the ventral compartment of the same wing disc (Supplementary Material, Fig. S4B). These data indicate that the severe loss-of-function phenotypes of *dre4* mutant flies may not be exclusively due to reduced ecdysone production. Instead, loss of *dre4* leads to increased cell apoptosis,

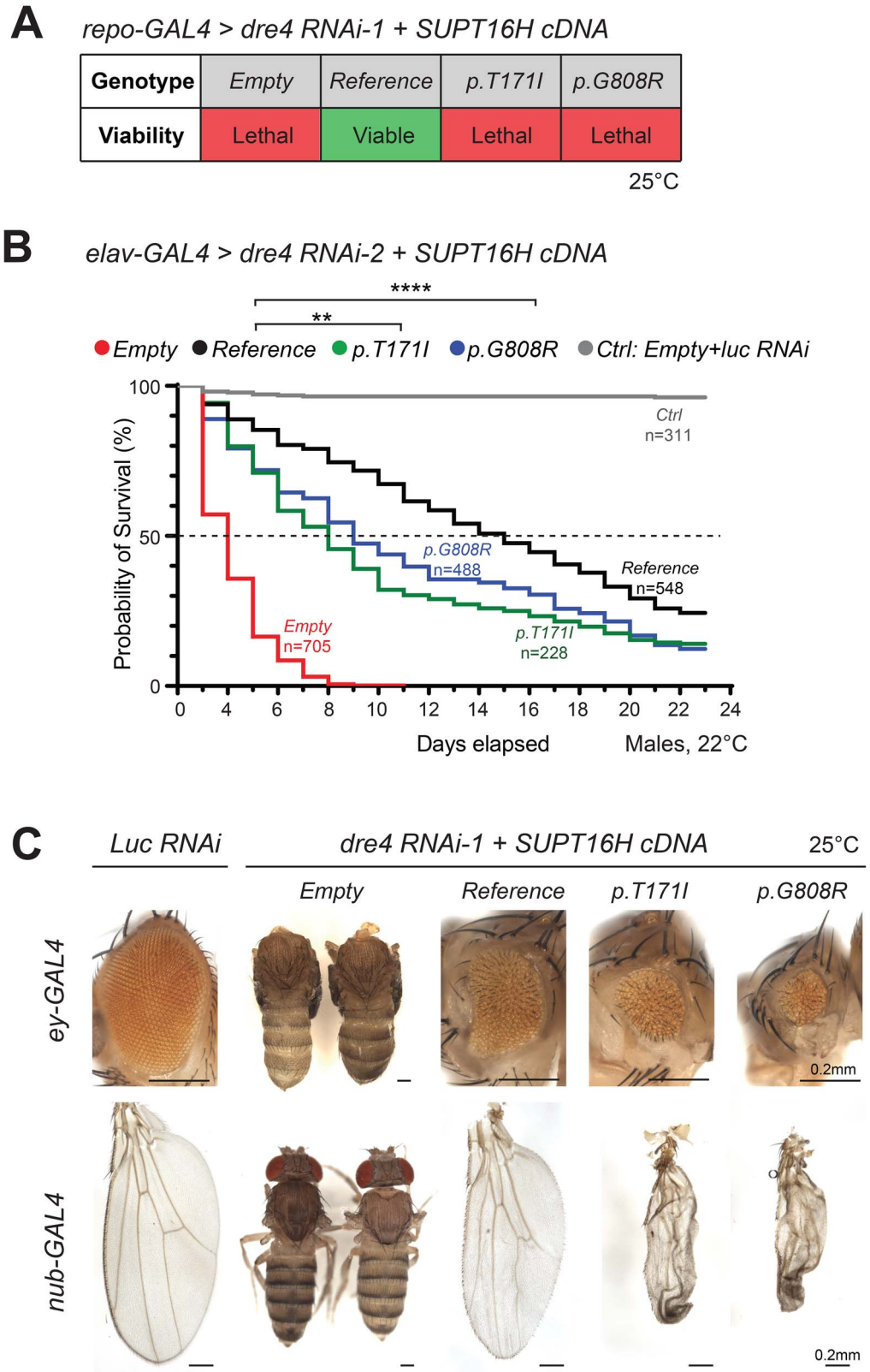

Figure 3. Loss of *dre4* causes severe phenotypes in multiple tissues that can be rescued by the *SUPT16H* reference cDNA but less effectively so by the two variant cDNAs. (**A**) Glia expression of *dre4 RNAi-1* causes lethality that can be fully rescued by co-expressing the *SUPT16H* reference cDNA, but is not rescued by expressing the variants. *UAS-Empty* is used as a negative control in all the following experiments and figures. (**B**) Neuronal expression of *dre4 RNAi-2* causes reduced life span, which can be partially rescued by co-expressing *SUPT16H* reference cDNA, but less efficiently so by the variants. The number of flies tested for each genotype is indicated. (**C**) Expressing *dre4 RNAi-2* in the eye (upper panel) or wing (lower panel) of the flies causes a complete loss of the head or wing, respectively. Co-expressing the *SUPT16H* reference cDNA strongly but not fully rescues the phenotype. However, co-expressing the variant cDNAs show less efficient rescue ability. Scale bar, 0.2 mm.

A

29°C		Relative frequency of progeny (Expected to be 0.5)		
Genotype		*Tub-GAL4*	*Act-GAL4 (III)*	*da-GAL4*
UAS-SUPT16H cDNA	*Empty*	0.51	0.62	0.50
	Reference	0.54	0.49	0.47
	p.T171I	0.49	0.48	0.52
	p.G808R	0.56	0.59	0.49

Cross strategy: *Tub-GAL4 / TM6B* x *UAS-SUPT16H cDNA*
Act-GAL4 / TM6B x *UAS-SUPT16H cDNA*
da-GAL4 x *UAS-SUPT16H cDNA / CyO*

B

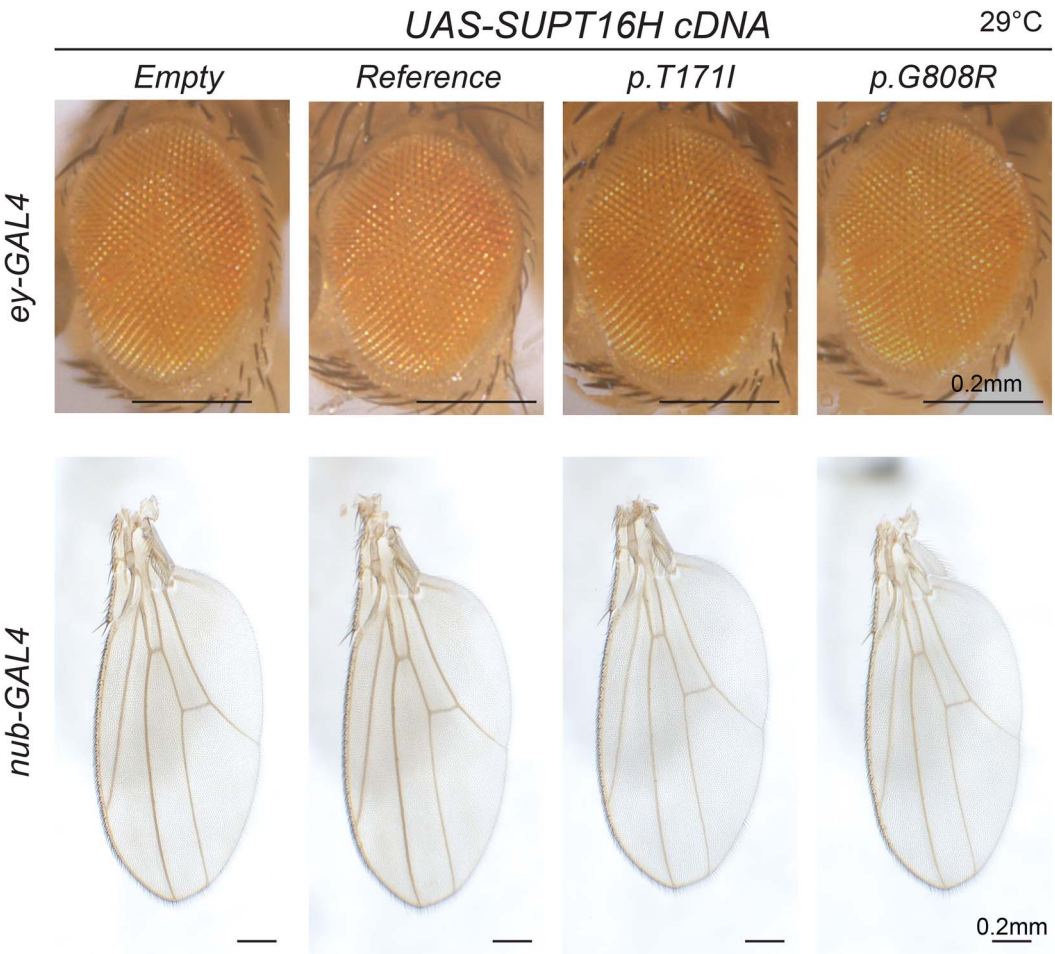

Figure 4. Ectopic expression of *SUPT16H* cDNAs in flies does not cause toxic effects. (**A**) Fly progeny that ubiquitously express *SUPT16H* reference or variant cDNAs are viable as adults. The crosses are listed under the table. Based on the Mendelian ratios, the expected frequency of the progeny carrying both *GAL4* and *UAS-SUPT16H cDNA* is 0.5. (**B**) Ectopic expression of *SUPT16H cDNAs* in eyes (upper panel) or wings (lower panel) does not cause morphological defects.

and the developmental defects in multiple tissues are likely to contribute to the lethality at an early stage.

To establish that *dre4* functions cell autonomously, we employed the flippase-out clone strategy (56) that permits the removal of *dre4* in random cells to allow comparison between *dre4* knockdown cells and neighboring wild-type cells within the same tissue. In the absence of a heat shock, there is leaking flippase activity that is sufficient to produce some GAL4 to drive the knockdown of *dre4* in a few cells. We focused on larval fat body cells, large flat cells of uniform size that are commonly used for flippase-out clone analysis at single-cell resolution. Immunofluorescent staining showed that the *dre4* knockdown cells (GFP positive) barely produce Dre4 protein (Fig. 5C), further validating that *dre4 RNAi* lines knock down the gene efficiently. Notably, these cells are much smaller than the neighboring wild-type cells, clearly showing that *dre4* is autonomously required for growth of these cells (Fig. 5C). The cell size reduction phenotype can be fully rescued by expression of the human reference *SUPT16H* but is only partially rescued by the variants identified in the probands (Fig. 5D and 5E), again supporting that the variants are loss-of-function alleles.

Discussion

Here we report two unrelated individuals with *de novo* missense variants in *SUPT16H*, a gene encoding the large subunit of the nucleosome organizer FACT complex. Both individuals have GDD, ID, seizures, structural abnormalities in the brain and some facial malformation.

SUPT16H localizes to 14q11.2. The microdeletion of chromosome region at 14q11-q22 is associated with a syndrome characterized by a spectrum of symptoms including developmental delay, cognitive impairment, autism, abnormal head size and facial dysmorphism (MIM: 613457) (57–61). The deletion of chromosome 14q11.2 ranges from 100 kb to >1 Mb, with a minimal common deletion region of ∼35 kb that covers only two genes, *SUPT16H* and *CHD8* (58). Which gene accounts for the symptoms is not obvious. Disruptive variants of *CHD8*, a gene encoding a chromatin remodeling factor, have been mainly associated with autism spectrum disorder and macrocephaly (62–64) and loss of function of *chd8* in zebrafish also recapitulated increased head size features of the human phenotype (62). Given that *SUPT16H* probands display overlapping symptoms with the 14q11-q22 deletion syndrome, including delayed gross and cognitive development, facial dysmorphism, congenital heart defects, as well as abnormal brain structure and seizures, it is possible that the phenotypes caused by the deletion are likely due to haploinsufficiency of both genes.

Although *in vitro* studies of *SUPT16H* and its orthologs have defined their biochemical properties, the *in vivo* functions of *SUPT16H* and its orthologs are less well studied at the organismal level, mainly because of the early lethality caused by the loss of the gene(s) in several species. In this study, taking advantage of tissue-specific RNAi-mediated knockdown, we reveal the functional requirement of *dre4* and show that it is required for the development of multiple tissues, including the nervous system, wing and eye. Also, the requirement of *dre4* varies in different types of glia. This observation indicates that different tissues and cells have different sensitivity to the level of *dre4*. Early studies in flies suggested that *dre4* loss affects ecdysone production in ring glands and that this loss causes developmental arrest, arguing for an endocrine mechanism of *dre4* through control of ecdysone production. However, we show that *dre4* is expressed in most or all tissues and that it is essential for cell survival, including the ring gland. We further show that *dre4* acts in a cell-autonomous manner in fat body cells using flippase-out clone analysis. Loss of *dre4* causes a very severe cell size reduction in the cells expressing *dre4 RNAi* but does not affect neighboring cells. Based on its broad expression and essential role in cell growth and survival across tissues, our data show that *SUPT16H/dre4* acts cell-autonomously.

Our data show that expression of the human *SUPT16H* reference cDNA is capable of suppressing most of the phenotypes associated with the loss of *dre4* in fly. In contrast, the variants are less efficient in rescuing the loss-of-function phenotypes, arguing that they are partial loss-of-function mutations. In addition, the ectopic overexpression assay suggests that the variants are less likely to have a dominant-negative or gain-of-function effect. In summary, our data indicate that the two *de novo* variants of *SUPT16H* (p.T171I and p.G808R) are disease-causing and provide compelling *in vivo* evidence that *SUPT16H* is associated with NDDs.

Materials and Methods

Next generation sequencing and human genetics analyses

Whole genome sequencing of the probands and data analyses were performed at the clinical sites. Firstly, cutadapt (65) (v1.15) was used to trim adaptor sequences at the tail of sequencing reads, and the sequencing reads were aligned to human reference genome (UCSC hg19) with BWA (66) (v0.7.15). Duplicated reads were marked by Picard (v2.4.1). Qualimap (67) (v2.2.1) was used to calculate base quality metrics, genome mapping rate and the coverage of targeted regions. Base quality score recalibration, indel realignment and variant (SNVs and InDels) calling were performed following the best practice protocol of the Genome Analysis Toolkit (68) (GATK, v3.8). Variant filtering was done by a finely tuned in house script. Pass-filter variants were annotated using the Pubvar variant annotation engine and VEP (69) (release 88). Variants that fit the dominant and recessive inheritance models were separately identified. Variants meeting any of the following criteria were excluded from genetic analysis: maximum population frequency was large than 0.01, genotype confidence was low or the variants were predicted as benign by all five algorithms (SIFT (70), PolyPhen 2 (71), MetaSVM (72), MCAP (73) and MutationTaster (74)). The pathogenic evidence of candidate disease-causing variants were scored by InterVar (75) (1.0.8) according to ACMG guidelines (76). All the above analyses were performed on Seqmax.

Fly stocks and maintenance

The fly strains used in this study were either generated in house or obtained from the Bloomington Drosophila Stock Center (BDSC). All the flies were reared on standard fly food and were cultured at room temperature unless specified. The fly stocks are listed:

y^{1}, *v*^{1}; *P{TKO.GS04655}attP40* (BDSC_80846)

w;P{GAL4-nos.NGT}40; P{UAS-Cas9.P2}attP2* (BDSC_67083)

dre4^{KO1} (generated in this study)

w^{1118}; *Df(3L)Exel6088, P{XP-U}Exel6088/TM6B, Tb*^{1} (BDSC_7567)

w^{1118}; *Dp(3;2)GV-CH321-36E03, PBac{GV-CH321-36E03}VK00037/CyO* (BDSC_90150)

UAS-SUPT16H^{Reference}*-VK37* (generated in this study)

UAS-SUPT16H^{T171I}*-VK37* (generated in this study)

UAS-SUPT16H^{G808R}*-VK37* (generated in this study)

UAS-Empty vector-VK37The inserted (generated in house) is in regular front, not in italic (ARC-EM), Nottingham UK

y^{1} *sc** *v*^{1} *sev*^{21}; *P{TRiP.GL00017}attP2* (BDSC_35149)

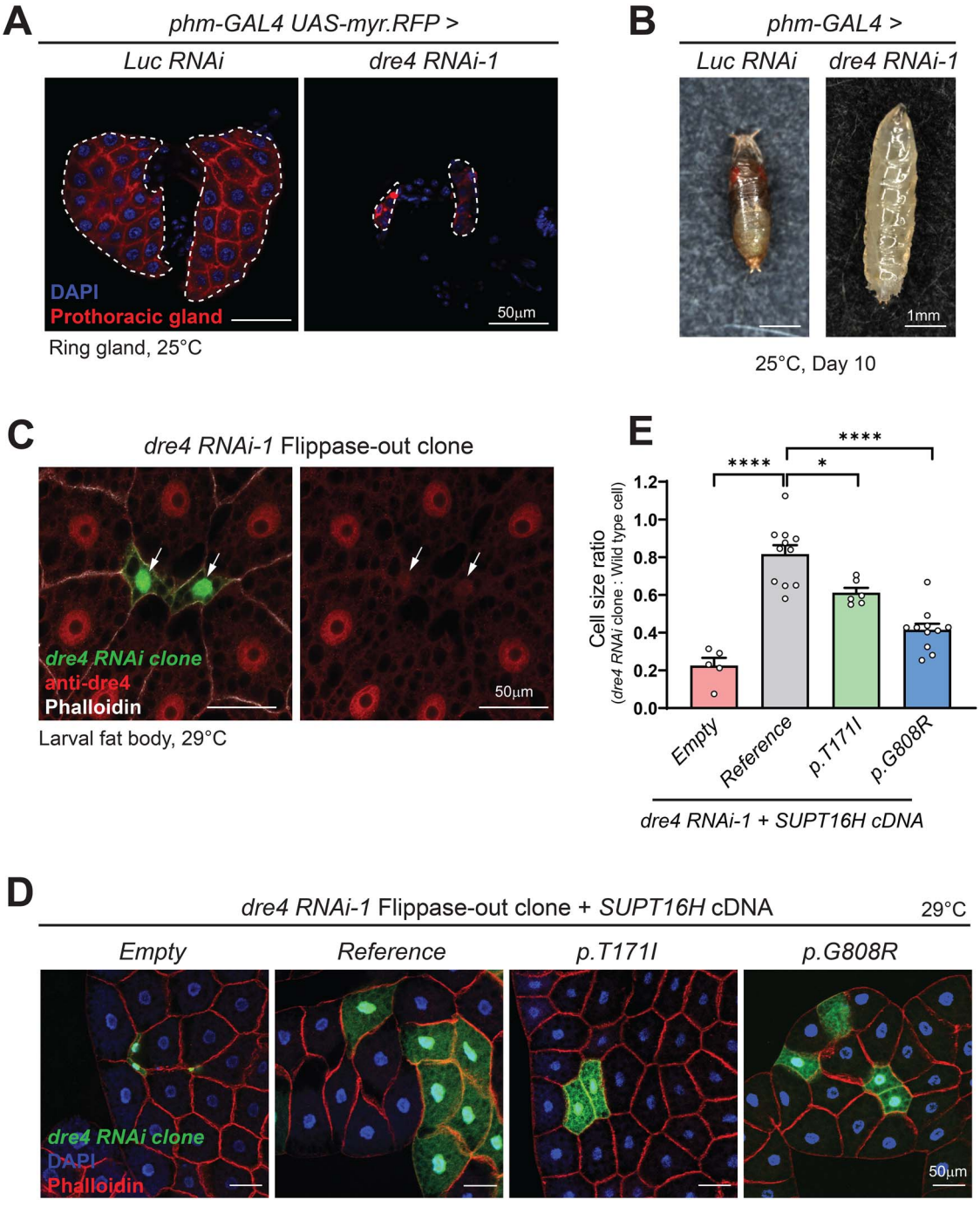

Figure 5. *dre4* functions in a cell-autonomous fashion. (**A**) Expression of *dre4 RNAi-1* in the prothoracic gland of ring gland (driven by *phm-GAL4*, the expression region is outlined by myr.RFP in red) impairs normal development of the prothoracic gland. Nuclei are labeled by DAPI (blue). Scale bar, 50 μm. (**B**) Expression of *dre4 RNAi-1* in the ring gland leads to developmental arrest at the L3 stage. Note that normal age-matched flies develop into dark pupae and eclose at day 10 when raised at 25°C (left panel). *phm-GAL4 > UAS-dre4 RNAi-1* flies are arrested as L3 and fail to properly pupate and eclose (right panel). Scale bar, 1 mm. (**C**) Representative confocal image of fat body flippase-out clones stained with antibody against Dre4 (red). Cell clones expressing *dre4 RNAi-1* are labeled with GFP (green). Note that the cells expressing *dre4 RNAi* (white arrow) have reduced Dre4 and are much smaller in size than surrounding cells. Cell outlines are indicated by Phalloidin (white). Scale bar, 50 μm. (**D**) Representative confocal images showing the rescuing of cell size by co-expressing *SUPT16H* cDNA in *dre4 RNAi-1* clones (green). Co-expression of the *SUPT16H* reference cDNA rescues cell size more efficiently than the variants. Cell outlines are indicated by Phalloidin (red). Nuclei are labeled by DAPI (blue). Scale bar, 50 μm. (**E**) Quantification of fat body cell size. Each point in the graph represents one confocal image randomly taken from larval fat body samples. For each image, cell size of the *dre4 RNAi-1* clones (green) and the wild-type cells surrounding the clones were measured, and the mean value of the cell size was used for ratio calculation. More than three larvae were dissected for each genotype. Unpaired *t* test, $^{*}P < 0.05$, $^{****}P < 0.0001$, mean ± SEM.

y^1 *sc** v^1 sev^{21}; *P{TRiP.HMS01332}attP2* (BDSC_34344)
y^1 v^1; *P{y[+t7.7] v[+t1.8] = TRiP.JF01355}attP2* (BDSC_31603)
y^1 *w**; *P{tubP-GAL4}LL7/TM3*, Sb^1 Ser^1 (BDSC_5138)
y^1 *w**; *P{Act5C-GAL4}17bFO1/TM6B*, Tb^1 (BDSC_3954)
*w**; *P{GAL4-da.G32}UH1*, Sb^1/*TM6B*, Tb^1 (BDSC_55851)
y^1 *w**; *P{Act5C-GAL4}25FO1/CyO*, y^+ (BDSC_4414)
w^{1118}; *P{GAL4}repo/TM3*, Sb^1 (BDSC_7415)
P{GAL4- elav.L}2/CyO (BDSC_8765)
*w**; *P{nub-GAL4.K}2* (BDSC_86108)
*w**; *P{nrv2-GAL4.S}3*; *P{nrv2-GAL4.S}8* (BDSC_6797)
*w**; *M{Tret1-1-GAL4.S}ZH-86Fb/TM6B*, Tb^1 (BDSC_94539)
*w**; *P{moody-GAL4.SPG}2* (BDSC_90883)
*w**; *P{GAL4-ey.H}3-8* (BDSC_5534)
w^{1118} *P{GawB-ΔKE}*$Bx^{MS1096-KE}$ (BDSC_8696)
w^{1118}; *P{UAS-myr-mRFP}2/TM6B*, Tb^1 (BDSC_7119)
y^1 *w**; *P{phm-GAL4.O}22* (BDSC_80577)
hsFlp; UAS-Dcr-2; Act > CD2 > Gal4, UAS-GFP/TM6B (77)

Generation of *dre4*^{KO1} allele

The *dre4*^{KO1} allele was generated using CRISPR/Cas9 genome engineering technology as previously described (40). Briefly, a *dre4 TKO* transgenic line carrying a single-guide RNA (sgRNA) is available from stock center (BDSC_80846) (78). The designed sgRNA (ACGCCTCTACACGGAATGGA) targets the first exon in both *dre4* isoforms. *dre4 TKO* flies were crossed to *nos-Cas9* transgenic flies. The first generation (F1) of male progeny carrying sgRNA and Cas9 were then crossed to third chromosome balancer flies *y w; Dr/TM6C, Sb, Tb*. Single F2 males were crossed to *y w; Dr/TM6C, Sb, Tb* to establish ∼10 individual stocks with potential indel mutations. We crossed out *nos-Cas9* and sgRNA transgene (both marked by y^+) by selecting y^- flies. Heterozygous F2 parent male or F3 progeny were screened for indel mutation by performing single fly genomic PCR using primer pairs flanking the targeted genome region, followed by Sanger sequencing of unpurified PCR product. Indel prediction from sequencing chromatograms was performed by Inference of CRISPR Edits (ICE) analysis. Several indel mutants were isolated and one with an early stop codon in the second exon, designated as *dre4*^{KO1}, was used in this study.

Measurement of survival ratio

To measure the survival ratio, heterozygous *Tub-GAL4/TM6B* or *Act-GAL4/TM6B* flies were crossed to homozygous *UAS-SUPT16H cDNA* flies; homozygous *da-GAL4* flies were crossed to heterozygous *UAS-SUPT16H cDNA/CyO* flies. The expected Mendelian ratio is 0.5 for the three crosses. The number of progeny for each genotype was counted, and the survival ratio was calculated.

Generation of *dre4 RNAi* flippase-out clone

dre4 RNAi clones in fat body were generated by crossing *UAS-dre4 RNAi* strains to *hsFlp; UAS-Dcr-2; Act > CD2 > Gal4, UAS-GFP/TM6B* (77). The *CD2* cassette is flanked by FRT sites and is inserted in between *Actin* promoter and *GAL4* sequence, preventing the expression of *GAL4*. The flies were kept at 29°C to induce spontaneous Flippase expression that removes the *CD2* insert to activate *Act-GAL4* expression and drive knockdown of *dre4* in GFP-marked cells.

Generation of *UAS-SUPT16H* reference and variant transgenic lines

UAS-SUPT16H reference and variant transgenic flies were generated as previously described (79). Briefly, *SUPT16H* reference cDNA coding sequence (CDS) was synthesized and ordered from GenScript (Clone ID: OHu64837D, ORF clones Accession NO: XM_011536381). *SUPT16H* cDNA CDS were first subcloned into the Gateway compatible entry vector pDONR223 by BP cloning (BP clonase II, Thermo Fisher Scientific, Nottingham UK) and sequentially into the destination vector pGW-attB-HA by LR cloning (LR clonase II, Thermo Fisher Scientific #11791100) (80). The *UAS-SUPT16H*^{T171I} and *UAS-SUPT16H*^{G808R} were generated by site-directed mutagenesis (PCR kit: iProof™ High-Fidelity DNA Polymerase, BIORAD #1725301; Mutagenesis template digestion: *DpnI* restriction enzyme, NEB # R0176L) and fully sequenced (Sanger).

The following primers (5′-3′) were used.

To clone *SUPT16H* CDS into entry vector:

*SUPT16H*_attB1_Fw: GGGGACAAGTTTGTACAAAAAAGCAGGCTTAATGGCTGTGACTCTGGACAAAGAC

*SUPT16H*_attB2_Rv: GGGGACCACTTTGTACAAGAAAGCTGGGTTTTACTTCCTCTTTTTCTTGGGGGGT

To generate T171I point mutation:

*SUPT16H*_T171I_Fw: GTTGTGGCATATATCATCGCTGTAAAGGAGGATG

*SUPT16H*_T171I_Rv: CTTTACAGCGATGATATATGCCACAACTGCACTG

To generate G808R point mutation:

*SUPT16H*_G808R_Fw: CTTGGGATTTAACAGAGCTCCCTATAGGAG

*SUPT16H*_G808R_Rv: CTATAGGGAGCTCTGTTAAATCCCAAGTCCC

Sanger Verification M13_F: GTAAAACGACGGCCAG

Sanger Verification *SUPT16H*_S1: CACTTTGGGGCTATCACTTG

Sanger Verification *SUPT16H*_S2: CAGCAGATTCAGAAAGCTCG

Sanger Verification *SUPT16H*_S3: GAAGCGGCACACGGATGTGC

Sanger Verification M13_R: CAGGAAACAGCTATGAC

All constructs were inserted into the VK37 (*PBac{y[+]-attP}VK00037*) docking site by ϕC31-mediated transgenesis (44).

Immunohistochemistry and confocal microscopy

Larval tissues were dissected in 1× PBS, fixed in 4% paraformaldehyde for 20 min at room temperature, washed in PBS (3 × 10 min), blocked in PBT–BSA (0.1% Triton X-100 detergent, 1% BSA in PBS), incubated in the primary antibody (Rabbit anti-dre4, 1:1000, gift from Dr Conaway (81)) solution in PBT–BSA at 4°C overnight, washed in 0.1% PBT (3 × 10 min), incubated with secondary antibody (1:200, goat anti-Rabbit; conjugated to Alexa 488 or Cy3, Jackson ImmunoResearch #111–545-003 and #111–165-144, respectively) for 2 h at room temperature (avoid from light) and washed in 0.1% PBT (3 × 10 min). Phalloidin (1:100, 647 nm, Invitrogen #A22287) was added in the secondary antibody solution. Stained tissues were mounted in DAPI-Vectashield (Vector Labs #H1200). For the experiments without antibody staining, phalloidin were diluted in 0.1% PBT. The images were captured using a confocal microscope (Leica SP8) and processed using ImageJ-FIJI software.

Imaging of adult fly wing and eye

For the imaging of the wings of adult flyies, the wing blades were dissected and mounted in a glycerol/ethanol 1/1 mixture. Only the wings of females were used. For the imaging of the eyes of adult flies, the flies were frozen to death at −20°C and glued on a slide with double-side sticky tape. The samples were imaged using bright field Stereomicroscope (Leica MZ16) and processed using ImageJ-FIJI software.

Real-time PCR

Real-time PCR was performed as previously described (82) with the following changes: All-In-One 5X RT MasterMix (abm#G592), iTaq Universal SYBR Green Master Mix (BioRad#1725120) and a BioRad C1000 Touch Cycler were used.

The following primers (5′-3′) were used.

*rp49*_D.mel_Fw: TGTCCTTCCAGCTTCAAGATGACCATC
*rp49*_D.mel_Rv: CTTGGGCTTGCGCATTTGTG
*dre4*_RT-PCR_Fw: GGCCACCATTTGTCATCACG
*dre4*_RT-PCR_Rv: ATGTCGCAGGAGTTGAGCC

Web resources

1000 Genomes, http://www.internationalgenome.org/
CADD, https://cadd.gs.washington.edu/
ClinVar, https://www.ncbi.nlm.nih.gov/clinvar/
dbSNP, https://www.ncbi.nlm.nih.gov/projects/SNP/
DECIPHER, https://decipher.sanger.ac.uk/
DGV, http://dgv.tcag.ca/dgv/app/home
DIOPT, https://www.flyrnai.org/cgi-bin/DRSC_orthologs.pl
ExAC, http://exac.broadinstitute.org/
gnomAD Browser, https://gnomad.broadinstitute.org
HUGO Gene Nomenclature Committee, https://www.genenames.org/
Human reference genome (UCSC hg19), https://genome.ucsc.edu
IMPC, https://www.mousephenotype.org/
Inference of CRISPR Edits (ICE) analysis, https://www.synthego.com/
InterVar, http://wintervar.wglab.org
MARRVEL, http://marrvel.org
M-CAP, http://bejerano.stanford.edu/mcap/
MutationTaster, https://www.mutationtaster.org/
OMIM, https://omim.org/
Picard Toolkit, https://broadinstitute.github.io/picard/
PolyPhen-2, http://genetics.bwh.harvard.edu/pph2/
PROVEAN, http://provean.jcvi.org/
Pubvar variant annotation engine, www.pubvar.com
RefSeq, https://www.ncbi.nlm.nih.gov/refseq/
SIFT, http://sift.jcvi.org
Seqmax, www.seqmax.com

Supplementary Material

Supplementary Material is available at *HMG* online.

Acknowledgements

We thank the probands and families for their participation in this study. We thank Bellen lab members for discussion and suggestions. Particularly, we thank Dr Liping Wang, Dr Zelha Nil, Dr Matthew Moulton and Dr Oguz Kanca for suggestions. We thank Dr Joan Conaway for the Dre4 antibody, and the Bloomington Drosophila Stock Center for providing stocks.

Conflict of Interest Statement. The authors declare no competing interests.

Funding

Neurological Research Institute; the Howard Hughes Medical Institute; The Office of Research Infrastructure Programs of the National Institutes of Health under the award numbers R24OD022005 to H.J.B and S.Y. The Huffington Foundation to H.J.B.; National Natural Science Foundation of China (No. 82171840) to H.G.; Natural Science Foundation Project of Chongqing (cstc2021jcyjmsxmX0281) to H.G.; The National Key Research and Development Program of China (2021YFC1005300 to H.W. and B.X.); H.C. is supported by the Warren Alpert Foundation.

References

1. Leo, L. and Romano, N.C. (2021) Emerging single-cell technological approaches to investigate chromatin dynamics and centromere regulation in human health and disease. *Int. J. Mol. Sci.*, **22**, 8809.
2. Sexton, T., Schober, H., Fraser, P. and Gasser, S.M. (2007) Gene regulation through nuclear organization. *Nat. Struct. Mol. Biol.*, **14**, 1049–1055.
3. Jiang, C. and Pugh, B.F. (2009) Nucleosome positioning and gene regulation: advances through genomics. *Nat. Rev. Genet.*, **10**, 161–172.
4. Choo, K.-B. (2011) Epigenetics in disease and cancer. *Malays. J. Pathol.*, **33**, 61–70.
5. Sananbenesi, F. and Fischer, A. (2009) The epigenetic bottleneck of neurodegenerative and psychiatric diseases. *Biol. Chem.*, **390**, 1145–1153.
6. Gabriele, M., Tobon, A.L., D'Agostino, G. and Testa, G. (2018) The chromatin basis of neurodevelopmental disorders: rethinking dysfunction along the molecular and temporal axes. *Prog. Neuropsychopharmacol. Biol. Psychiatry.*, **84**, 306–327.
7. van Bokhoven, H. (2011) Genetic and epigenetic networks in intellectual disabilities. *Annu. Rev. Genet.*, **45**, 81–104.
8. Timpano, S. and Picketts, D.J. (2020) Neurodevelopmental disorders caused by defective chromatin remodeling: phenotypic complexity is highlighted by a review of ATRX function. *Front. Genet.*, **11**, 885.
9. Sokpor, G., Xie, Y., Rosenbusch, J. and Tuoc, T. (2017) Chromatin remodeling BAF (SWI/SNF) complexes in neural development and disorders. *Front. Mol. Neurosci.*, **10**, 243.
10. Hoffmann, A. and Spengler, D. (2019) Chromatin remodeling complex NuRD in neurodevelopment and neurodevelopmental disorders. *Front. Genet.*, **10**, 682.
11. Orphanides, G., LeRoy, G., Chang, C.-H., Luse, D.S. and Reinberg, D. (1998) FACT, a factor that facilitates transcript elongation through nucleosomes. *Cell*, **92**, 105–116.
12. Belotserkovskaya, R., Oh, S., Bondarenko, V.A., Orphanides, G., Studitsky, V.M. and Reinberg, D. (2003) FACT facilitates transcription-dependent nucleosome alteration. *Science*, **301**, 1090–1093.
13. Wang, J., Al-Ouran, R., Hu, Y., Kim, S.-Y., Wan, Y.-W., Wangler, M.F., Yamamoto, S., Chao, H.-T., Comjean, A., Mohr, S.E. *et al.* (2017) MARRVEL: integration of human and model organism genetic resources to facilitate functional annotation of the human genome. *Am. J. Hum. Genet.*, **100**, 843–853.
14. Hu, Y., Flockhart, I., Vinayagam, A., Bergwitz, C., Berger, B., Perrimon, N. and Mohr, S.E. (2011) An integrative approach to ortholog prediction for disease-focused and other functional studies. *BMC Bioinformatics*, **12**, 357.
15. Kemble, D.J., McCullough, L.L., Whitby, F.G., Formosa, T. and Hill, C.P. (2015) FACT disrupts nucleosome structure by binding h2a-h2b with conserved peptide motifs. *Mol. Cell*, **60**, 294–306.
16. Mayanagi, K., Saikusa, K., Miyazaki, N., Akashi, S., Iwasaki, K., Nishimura, Y., Morikawa, K. and Tsunaka, Y. (2019) Structural visualization of key steps in nucleosome reorganization by human FACT. *Sci. Rep.*, **9**, 10183.
17. Gurova, K., Chang, H.-W., Valieva, M.E., Sandlesh, P. and Studitsky, V.M. (2018) Structure and function of the histone chaperone

FACT—resolving FACTual issues. *Biochim. Biophys. Acta*, **1861**, 892–904.
18. Stuwe, T., Hothorn, M., Lejeune, E., Rybin, V., Bortfeld, M., Scheffzek, K. and Ladurner, A.G. (2008) The FACT Spt16 "peptidase" domain is a histone H3–H4 binding module. *Proc. Natl. Acad. Sci. U. S. A.*, **105**, 8884–8889.
19. Wang, T., Liu, Y., Edwards, G., Krzizike, D., Scherman, H. and Luger, K. (2018) The histone chaperone FACT modulates nucleosome structure by tethering its components. *Life Sci. Alliance.*, **1**, e201800107.
20. Okuhara, K., Ohta, K., Seo, H., Shioda, M., Yamada, T., Tanaka, Y., Dohmae, N., Seyama, Y., Shibata, T. and Murofushi, H. (1999) A DNA unwinding factor involved in DNA replication in cell-free extracts of Xenopus eggs. *Curr. Biol.*, **9**, 341–351.
21. Malone, E.A., Clark, C.D., Chiang, A. and Winston, F. (1991) Mutations in SPT16/CDC68 suppress cis- and trans-acting mutations that affect promoter function in *Saccharomyces cerevisiae*. *Mol. Cell. Biol.*, **11**, 5710–5717.
22. Chen, P., Dong, L., Hu, M., Wang, Y.-Z., Xiao, X., Zhao, Z., Yan, J., Wang, P.-Y., Reinberg, D., Li, M. *et al.* (2018) Functions of FACT in breaking the nucleosome and maintaining its integrity at the single-nucleosome level. *Mol. Cell*, **71**, 284–293.e4.
23. Bina, R., Matalon, D., Fregeau, B., Tarsitano, J.J., Aukrust, I., Houge, G., Bend, R., Warren, H., Stevenson, R.E., Stuurman, K.E. *et al.* (2020) De novo variants in SUPT16H cause neurodevelopmental disorders associated with corpus callosum abnormalities. *J. Med. Genet.*, **57**, 461–465.
24. Hamanaka, K., Miyake, N., Mizuguchi, T., Miyatake, S., Uchiyama, Y., Tsuchida, N., Sekiguchi, F., Mitsuhashi, S., Tsurusaki, Y., Nakashima, M. *et al.* (2022) Large-scale discovery of novel neurodevelopmental disorder-related genes through a unified analysis of single-nucleotide and copy number variants. *Genome. Med.*, **14**, 40.
25. Dickinson, M.E., Flenniken, A.M., Ji, X., Teboul, L., Wong, M.D., White, J.K., Meehan, T.F., Weninger, W.J., Westerberg, H., Adissu, H. *et al.* (2016) High-throughput discovery of novel developmental phenotypes. *Nature*, **537**, 508–514.
26. Espanola, S.G., Song, H., Ryu, E., Saxena, A., Kim, E.-S., Manegold, J.E., Nasamran, C.A., Sahoo, D., Oh, C.-K., Bickers, C. *et al.* (2020) Haematopoietic stem cell-dependent Notch transcription is mediated by p53 through the Histone chaperone Supt16h. *Nat. Cell Biol.*, **22**, 1411–1422.
27. Sliter, T. and Gilbert, L. (1992) Developmental arrest and ecdysteroid deficiency resulting from mutations at the dre4 locus of Drosophila. *Genetics*, **130**, 555–568.
28. Sliter, T.J., Henrich, V.C., Tucker, R.L. and Gilbert, L.I. (1989) The genetics of the Dras3-roughened-ecdysoneless chromosomal region (62B3-4 to 62D3-4) in *Drosophila melanogaster*: analysis of recessive lethal mutations. *Genetics*, **123**, 327–336.
29. Keller, D.M. and Lu, H. (2002) p53 Serine 392 phosphorylation increases after UV through induction of the assembly of the CK2·hSPT16·SSRP1 complex. *J. Biol. Chem.*, **277**, 50206–50213.
30. O'Donnell, A.F., Brewster, N.K., Kurniawan, J., Minard, L.V., Johnston, G.C. and Singer, R.A. (2004) Domain organization of the yeast histone chaperone FACT: the conserved N-terminal domain of FACT subunit Spt16 mediates recovery from replication stress. *Nucleic Acids Res.*, **32**, 5894–5906.
31. VanDemark, A.P., Blanksma, M., Ferris, E., Heroux, A., Hill, C.P. and Formosa, T. (2006) The structure of the yFACT Pob3-M domain, its interaction with the DNA replication factor RPA, and a potential role in nucleosome deposition. *Mol. Cell*, **22**, 363–374.
32. Orphanides, G., Wu, W.-H., Lane, W.S., Hampsey, M. and Reinberg, D. (1999) The chromatin-specific transcription elongation factor FACT comprises human SPT16 and SSRP1 proteins. *Nature*, **400**, 284–288.
33. Bondarenko, M.T., Maluchenko, N.V., Valieva, M.E., Gerasimova, N.S., Kulaeva, O.I., Georgiev, P.G. and Studitsky, V.M. (2015) Structure and function of histone chaperone FACT. *Mol. Biol.*, **49**, 796–809.
34. Kemble, D.J., Whitby, F.G., Robinson, H., McCullough, L.L., Formosa, T. and Hill, C.P. (2013) Structure of the Spt16 middle domain reveals functional features of the histone chaperone FACT. *J. Biol. Chem.*, **288**, 10188–10194.
35. Hondele, M., Stuwe, T., Hassler, M., Halbach, F., Bowman, A., Zhang, E.T., Nijmeijer, B., Kotthoff, C., Rybin, V., Amlacher, S. *et al.* (2013) Structural basis of histone H2A–H2B recognition by the essential chaperone FACT. *Nature*, **499**, 111–114.
36. Liu, Y., Zhou, K., Zhang, N., Wei, H., Tan, Y.Z., Zhang, Z., Carragher, B., Potter, C.S., D'Arcy, S. and Luger, K. (2019) FACT caught in the act of manipulating the nucleosome. *Nature*, **577**, 426–431.
37. Karczewski, K.J., Francioli, L.C., Tiao, G., Cummings, B.B., Alföldi, J., Wang, Q., Collins, R.L., Laricchia, K.M., Ganna, A., Birnbaum, D.P. *et al.* (2020) The mutational constraint spectrum quantified from variation in 141,456 humans. *Nature*, **581**, 434–443.
38. Şentürk, M. and Bellen, H.J. (2018) Genetic strategies to tackle neurological diseases in fruit flies. *Curr. Opin. Neurobiol.*, **50**, 24–32.
39. Bellen, H.J., Wangler, M.F. and Yamamoto, S. (2019) The fruit fly at the interface of diagnosis and pathogenic mechanisms of rare and common human diseases. *Hum. Mol. Genet.*, **28**, R207–R214.
40. Port, F., Chen, H.-M., Lee, T. and Bullock, S.L. (2014) Optimized CRISPR/Cas tools for efficient germline and somatic genome engineering in Drosophila. *Proc. Natl. Acad. Sci. U. S. A.*, **111**, E2967–E2976.
41. Port, F., Muschalik, N. and Bullock, S.L. (2015) Systematic evaluation of Drosophila CRISPR tools reveals safe and robust alternatives to autonomous gene drives in basic research. *G3. (Bethesda)*, **5**, 1493–1502.
42. Port, F. and Bullock, S.L. (2016) Augmenting CRISPR applications in Drosophila with tRNA-flanked sgRNAs. *Nat. Methods*, **13**, 852–854.
43. Parks, A.L., Cook, K.R., Belvin, M., Dompe, N.A., Fawcett, R., Huppert, K., Tan, L.R., Winter, C.G., Bogart, K.P., Deal, J.E. *et al.* (2004) Systematic generation of high-resolution deletion coverage of the *Drosophila melanogaster* genome. *Nat. Genet.*, **36**, 288–292.
44. Venken, K.J.T., He, Y., Hoskins, R.A. and Bellen, H.J. (2006) P[acman]: A BAC transgenic platform for targeted insertion of large DNA fragments in *D. melanogaster*. *Science*, **314**, 1747–1751.
45. Ni, J.-Q., Zhou, R., Czech, B., Liu, L.-P., Holderbaum, L., Yang-Zhou, D., Shim, H.-S., Tao, R., Handler, D., Karpowicz, P. *et al.* (2011) A genome-scale shRNA resource for transgenic RNAi in Drosophila. *Nat. Methods*, **8**, 405–407.
46. Carithers, L.J., Ardlie, K., Barcus, M., Branton, P.A., Britton, A., Buia, S.A., Compton, C.C., DeLuca, D.S., Peter-Demchok, J., Gelfand, E.T. *et al.* (2015) A novel approach to high-quality postmortem tissue procurement: the GTEx project. *Biopreserv. Biobank*, **13**, 311–319.
47. Volkenhoff, A., Weiler, A., Letzel, M., Stehling, M., Klämbt, C. and Schirmeier, S. (2015) Glial glycolysis is essential for neuronal survival in Drosophila. *Cell Metab.*, **22**, 437–447.
48. Stetina, J.R.V., Frawley, L.E., Unhavaithaya, Y. and Orr-Weaver, T.L. (2018) Variant cell cycles regulated by Notch signaling control cell size and ensure a functional blood-brain barrier. *Development*, **145**, dev157115.
49. Yeh, P.-A., Liu, Y.-H., Chu, W.-C., Liu, J.-Y. and Sun, Y.H. (2018) Glial expression of disease-associated poly-glutamine proteins

impairs the blood–brain barrier in Drosophila. *Hum. Mol. Genet.*, **27**, 2546–2562.
50. Winkler, B., Funke, D., Benmimoun, B., Spéder, P., Rey, S., Logan, M.A. and Klämbt, C. (2021) Brain inflammation triggers macrophage invasion across the blood-brain barrier in Drosophila during pupal stages. *Sci. Adv.*, **7**, eabh0050.
51. Coutinho-Budd, J.C., Sheehan, A.E. and Freeman, M.R. (2017) The secreted neurotrophin Spätzle 3 promotes glial morphogenesis and supports neuronal survival and function. *Genes Dev.*, **31**, 2023–2038.
52. Yamanaka, N., Rewitz, K.F. and O'Connor, M.B. (2013) Ecdysone control of developmental transitions: lessons from Drosophila research. *Annu. Rev. Entomol.*, **58**, 497–516.
53. Ono, H., Rewitz, K.F., Shinoda, T., Itoyama, K., Petryk, A., Rybczynski, R., Jarcho, M., Warren, J.T., Marqués, G., Shimell, M.J. *et al.* (2006) Spook and Spookier code for stage-specific components of the ecdysone biosynthetic pathway in Diptera. *Dev. Biol.*, **298**, 555–570.
54. Nakajima, Y., Lee, Z.T., McKinney, S.A., Swanson, S.K., Florens, L. and Gibson, M.C. (2019) Junctional tumor suppressors interact with 14-3-3 proteins to control planar spindle alignment. *J. Cell Biol.*, **218**, 1824–1838.
55. Yuva-Aydemir, Y., Almeida, S., Krishnan, G., Gendron, T.F. and Gao, F.-B. (2019) Transcription elongation factor AFF2/FMR2 regulates expression of expanded GGGGCC repeat-containing C9ORF72 allele in ALS/FTD. *Nat. Commun.*, **10**, 5466.
56. Germani, F., Bergantinos, C. and Johnston, L.A. (2018) Mosaic analysis in Drosophila. *Genetics*, **208**, 473–490.
57. Terrone, G., Cappuccio, G., Genesio, R., Esposito, A., Fiorentino, V., Riccitelli, M., Nitsch, L., Brunetti-Pierri, N. and Giudice, E.D. (2014) A case of 14q11.2 microdeletion with autistic features, severe obesity and facial dysmorphisms suggestive of Wolf–Hirschhorn syndrome. *Am. J. Med. Genet. A*, **164**, 190–193.
58. Zahir, F., Firth, H.V., Baross, A., Delaney, A.D., Eydoux, P., Gibson, W.T., Langlois, S., Martin, H., Willatt, L., Marra, M.A. *et al.* (2007) Novel deletions of 14q11.2 associated with developmental delay, cognitive impairment and similar minor anomalies in three children. *J. Med. Genet.*, **44**, 556–561.
59. Yasin, H., Gibson, W.T., Langlois, S., Stowe, R.M., Tsang, E.S., Lee, L., Poon, J., Tran, G., Tyson, C., Wong, C. *et al.* (2019) A distinct neurodevelopmental syndrome with intellectual disability, autism spectrum disorder, characteristic facies, and macrocephaly is caused by defects in CHD8. *J. Hum. Genet.*, **64**, 271–280.
60. Shapira, S.K., Anderson, K.L., Orr-Urtregar, A., Craigen, W.J., Lupski, J.R. and Shaffer, L.G. (1994) De novo proximal interstitial deletions of 14q: cytogenetic and molecular investigations. *Am. J. Med. Genet.*, **52**, 44–50.
61. Grammatico, P., de Sanctis, S., di Rosa, C., Cupilari, F. and del Porto, G. (1994) First case of deletion 14q11.2q13: clinical phenotype. *Ann. Genet.*, **37**, 30–32.
62. Bernier, R., Golzio, C., Xiong, B., Stessman, H.A., Coe, B.P., Penn, O., Witherspoon, K., Gerdts, J., Baker, C., Vulto-van Silfhout, A.T. *et al.* (2014) Disruptive CHD8 mutations define a subtype of autism early in development. *Cell*, **158**, 263–276.
63. Barnard, R.A., Pomaville, M.B. and O'Roak, B.J. (2015) Mutations and modeling of the chromatin remodeler CHD8 define an emerging autism etiology. *Front. Neurosci.*, **9**, 477.
64. Neale, B.M., Kou, Y., Liu, L., Ma'ayan, A., Samocha, K.E., Sabo, A., Lin, C.-F., Stevens, C., Wang, L.-S., Makarov, V. *et al.* (2012) Patterns and rates of exonic de novo mutations in autism spectrum disorders. *Nature*, **485**, 242–245.
65. Martin, M. (2011) Cutadapt removes adapter sequences from high-throughput sequencing reads. *Embnet. J.*, **17**, 10–12.
66. Li, H. (2013) Aligning sequence reads, clone sequences and assembly contigs with BWA-MEM. *Arxiv: Genomics*, 1303.3997v2 [q-bio.GN], Preprintat https://arxiv.org/abs/1303.3997.
67. García-Alcalde, F., Okonechnikov, K., Carbonell, J., Cruz, L.M., Götz, S., Tarazona, S., Dopazo, J., Meyer, T.F. and Conesa, A. (2012) Qualimap: evaluating next-generation sequencing alignment data. *Bioinformatics*, **28**, 2678–2679.
68. Auwera, G.A., Carneiro, M.O., Hartl, C., Poplin, R., del Angel, G., Levy-Moonshine, A., Jordan, T., Shakir, K., Roazen, D., Thibault, J. *et al.* (2013) From FastQ data to high-confidence variant calls: the genome analysis toolkit best practices pipeline. *Curr. Protoc. Bioinformatics*, **43**, 11.10.1-11.10.33.
69. McLaren, W., Gil, L., Hunt, S.E., Riat, H.S., Ritchie, G.R.S., Thormann, A., Flicek, P. and Cunningham, F. (2016) The Ensembl variant effect predictor. *Genome Biol.*, **17**, 122.
70. Kumar, P., Henikoff, S. and Ng, P.C. (2009) Predicting the effects of coding non-synonymous variants on protein function using the SIFT algorithm. *Nat. Protoc.*, **4**, 1073–1081.
71. Adzhubei, I.A., Schmidt, S., Peshkin, L., Ramensky, V.E., Gerasimova, A., Bork, P., Kondrashov, A.S. and Sunyaev, S.R. (2010) A method and server for predicting damaging missense mutations. *Nat. Methods*, **7**, 248–249.
72. Kim, S., Jhong, J.-H., Lee, J. and Koo, J.-Y. (2017) Meta-analytic support vector machine for integrating multiple omics data. *Biodata. Min.*, **10**, 2.
73. Jia, P., Anderson, J.D., Leitner, M. and Rheingans, R. (2016) High-resolution spatial distribution and estimation of access to improved sanitation in Kenya. *PLoS One*, **11**, e0158490.
74. Schwarz, J.M., Rödelsperger, C., Schuelke, M. and Seelow, D. (2010) MutationTaster evaluates disease-causing potential of sequence alterations. *Nat. Methods*, **7**, 575–576.
75. Li, Q. and Wang, K. (2017) InterVar: clinical interpretation of genetic variants by the 2015 ACMG-AMP guidelines. *Am. J. Hum. Genet.*, **100**, 267–280.
76. Richards, S., Aziz, N., Bale, S., Bick, D., Das, S., Gastier-Foster, J., Grody, W.W., Hegde, M., Lyon, E., Spector, E. *et al.* (2015) Standards and guidelines for the interpretation of sequence variants: a joint consensus recommendation of the American College of Medical Genetics and Genomics and the Association for Molecular Pathology. *Genet. Med.*, **17**, 405–424.
77. Zheng, Y., Buchwalter, R.A., Zheng, C., Wight, E.M., Chen, J.V. and Megraw, T.L. (2020) A perinuclear microtubule-organizing centre controls nuclear positioning and basement membrane secretion. *Nat. Cell Biol.*, **22**, 297–309.
78. Zirin, J., Hu, Y., Liu, L., Yang-Zhou, D., Colbeth, R., Yan, D., Ewen-Campen, B., Tao, R., Vogt, E., VanNest, S. *et al.* (2020) Large-scale transgenic Drosophila resource collections for loss- and gain-of-function studies. *Genetics*, **214**, 755–767.
79. Kanca, O., Andrews, J.C., Lee, P.-T., Patel, C., Braddock, S.R., Slavotinek, A.M., Cohen, J.S., Gubbels, C.S., Aldinger, K.A., Williams, J. *et al.* (2019) De novo variants in WDR37 are associated with epilepsy, colobomas, dysmorphism, developmental delay, intellectual disability, and cerebellar hypoplasia. *Am. J. Hum. Genet.*, **105**, 413–424.
80. Bischof, J., Björklund, M., Furger, E., Schertel, C., Taipale, J. and Basler, K. (2013) A versatile platform for creating a comprehensive UAS-ORFeome library in Drosophila. *Development*, **140**, 2434–2442.
81. Tettey, T.T., Gao, X., Shao, W., Li, H., Story, B.A., Chitsazan, A.D., Glaser, R.L., Goode, Z.H., Seidel, C.W., Conaway, R.C. *et al.* (2019) A

role for FACT in RNA polymerase II promoter-proximal pausing. *Cell Rep.*, **27**, 3770–3779.e7.

82. Goodman, L.D., Cope, H., Nil, Z., Ravenscroft, T.A., Charng, W.-L., Lu, S., Tien, A.-C., Pfundt, R., Koolen, D.A., Haaxma, C.A. *et al.* (2021) TNPO2 variants associate with human developmental delays, neurologic deficits, and dysmorphic features and alter TNPO2 activity in Drosophila. *Am. J. Hum. Genet.*, **108**, 1669–1691.